'Trigger' Events Precede Calcium Puffs in *Xenopus* Oocytes

Heather J. Rose, Sheila Dargan, Jianwei Shuai, and Ian Parker
Department of Neurobiology and Behavior, University of California, Irvine, California 92697

ABSTRACT The liberation of calcium ions sequestered in the endoplasmic reticulum through inositol 1,4,5-trisphosphate receptors/channels (IP_3Rs) results in a spatiotemporal hierarchy of calcium signaling events that range from single-channel openings to local Ca^{2+} puffs believed to arise from several to tens of clustered IP_3Rs to global calcium waves. Using high-resolution confocal linescan imaging and a sensitive Ca^{2+} indicator dye (fluo-4-dextran), we show that puffs are often preceded by small, transient Ca^{2+} elevations that we christen "trigger events". The magnitude of triggers is consistent with their arising from the opening of a single IP_3 receptor/channel, and we propose that they initiate puffs by recruiting neighboring IP_3Rs within the cluster by a regenerative process of Ca^{2+}-induced Ca^{2+} release. Puff amplitudes (fluorescence ratio change) are on average ~6 times greater than that of the triggers, suggesting that at least six IP_3Rs may simultaneously be open during a puff. Trigger events have average durations of ~12 ms, as compared to 19 ms for the mean rise time of puffs, and their spatial extent is ~3 times smaller than puffs (respective widths at half peak amplitude 0.6 and 1.6 μm). All these parameters were relatively independent of IP_3 concentration, although the proportion of puffs showing resolved triggers was greatest (~80%) at low [IP_3]. Because Ca^{2+} puffs constitute the building blocks from which cellular IP_3-mediated Ca^{2+} signals are constructed, the events that initiate them are likely to be of fundamental importance for cell signaling. Moreover, the trigger events provide a useful yardstick by which to derive information regarding the number and spatial arrangement of IP_3Rs within clusters.

INTRODUCTION

Inositol 1,4,5-trisphosphate (IP_3) is a major intracellular messenger that functions by binding to IP_3 receptors/channels (IP_3Rs) to liberate Ca^{2+} ions sequestered in the endoplasmic reticulum (ER) (1). Opening of these channels is regulated not only by IP_3 but also biphasically by cytosolic Ca^{2+} itself, leading to a regenerative process of Ca^{2+}-induced Ca^{2+} release (CICR) (2–5). As a result of this positive feedback, in conjunction with the clustered organization of IP_3Rs in the ER membrane (6–8), cytosolic Ca^{2+} signals in many cell types display a hierarchical spatiotemporal organization, ranging from Ca^{2+} ''blips'' that represent putative openings of single IP_3Rs (9–11), through ''puffs'' that involve concerted openings of several clustered IP_3Rs (10–13), to saltatory Ca^{2+} waves that propagate globally across cells by successive cycles of CICR and Ca^{2+} diffusion between clusters (12,14).

Ca^{2+} puffs serve as the basic ''building blocks'' from which global Ca^{2+} signals (waves) are constructed (5,10,12, 14) and may also regulate local signaling functions in their own right. It is, therefore, important to understand the fundamental mechanisms by which they arise. However, several key questions remain unresolved: notably, the number of IP_3Rs/channels that open during a puff, the density and spatial distribution of these channels within a cluster, and the triggering mechanism by which the initial opening of one channel may rapidly induce the concerted opening of closely neighboring IP_3Rs within a cluster.

The *Xenopus* oocyte has proved a highly advantageous model cell system in which to study the elementary events of Ca^{2+} signaling by virtue of its large size and lack of ER Ca^{2+} release channels (e.g., ryanodine receptors (RyRs) and cADP-ribose receptors) other than IP_3Rs (15–19). Here, we have explored the microarchitecture of puffs in the oocyte at improved resolution, employing confocal linescan microscopy together with a high- dynamic range fluorescent Ca^{2+} indicator (fluo-4-dextran). A major finding is the discovery of novel IP_3-Ca^{2+} signaling events, which we christen Ca^{2+} ''triggers''. These are small, transient (~12 ms) Ca^{2+} elevations that arise at puff sites immediately preceding the onset of puffs. We interpret them as arising from the opening of a single IP_3R and propose that the resulting Ca^{2+} liberation acts as a trigger to induce an explosive concerted opening of multiple adjacent IP_3Rs to generate a puff. The Ca^{2+} triggers offer a useful yardstick by which to estimate the number of channels involved in a puff, and comparison of the spatial spread of trigger and puff Ca^{2+} signals provides information regarding the distribution of channels at a puff site. This work presents experimental findings on the spatiotemporal dynamics of triggers and puffs, and in an accompanying work (20) we use these experimental data in a mathematical simulation to predict the architecture of an IP_3R cluster.

MATERIALS AND METHODS

Preparation and microinjection of oocytes

Xenopus laevis were anesthetized by immersion in 0.17% MS-222 for 15 min and sacrificed by decapitation in accordance with protocols approved by the UC Irvine Animal Care and Use Committee. Stage V and VI oocytes

Submitted May 11, 2006, and accepted for publication August 30, 2006.

Address reprint requests to Heather Rose, Dept. of Neurobiology and Behavior, University of California, Irvine, CA 92697. Tel.: 949-824-7833; Fax: 949-824-2447; E-mail: heather@uci.edu.

Sheila Dargan's present address is Dept. of Anatomy, Bristol University, Bristol, UK.

0006-3495/06/12/4024/09 $2.00

doi: 10.1529/biophysj.106.088872

were manually plucked and then collagenase treated (0.5 mg/ml) for 30 min. Oocytes were stored in Barth's solution (in mM: NaCl, 88; KCl, 1; $NaHCO_3$, 2.4; $MgSO_4$, 0.82; $Ca(NO_3)_2$, 0.33; $CaCl_2$, 0.41; Hepes, 5; gentamicin, 0.1 mg/ml; at pH 7.4) for 1–4 days before use. A Drummond (Broomall, PA) microinjector was used to inject oocytes to final concentrations (assuming 1-μl cytosolic volume) of 25–40 μM fluo-4-dextran (low affinity, $K_d = \sim 3$ μM or high affinity, $K_d = 0.8$ μM: manufacturer's data), 8 μM caged IP_3 (D-myo-inositol 1,4,5-triphosphate, P4(5)-(10(2-nitrophenyl)ethyl) ester), and 90 μM or 300 μM EGTA. EGTA was used to functionally isolate puffs by inhibiting propagation of Ca^{2+} waves (21); puff characteristics were similar for the two buffer concentrations. After allowing >45 min for intracellular diffusion of compounds, oocytes were imaged using confocal linescan microscopy. The temporal and spatial characteristics of puffs collected with low- versus high-affinity fluo-4-dextrans were indistinguishable, although puff amplitudes were somewhat greater using the low-affinity version fluo-4-dextran (8.8 ± 0.33 $\Delta F/F_0$, $n = 75$ vs. 7.13 ± 0.30 $\Delta F/F_0$, $n = 37$; $p < 0.005$). Data from the low-affinity and high-affinity versions of the fluo-4-dextran are combined in the results; the majority of the results were obtained with the high-affinity version ($K_d = 0.8$ μM).

Calcium indicators and caged IP_3 were obtained from Invitrogen (Carlsbad, CA); all other reagents were from Sigma Chemical (St. Louis, MO).

Confocal linescan microscopy

Confocal calcium images were obtained using a custom-built linescan confocal scanner interfaced to an Olympus IX70 inverted microscope (Melville, NY) (22). Experiments were performed at room temperature in Ringer's solution (in mM: $NaCl_2$, 120; KCl, 2; $CaCl_2$, 1.8; Hepes, 5; pH 7.4). The microscope was focused in the granule layer of the animal hemisphere where IP_3R density and Ca^{2+} signals are maximal (6), and linescan images were acquired using custom routines written in Labview (National Instruments; Austin, TX). Temporal resolution was optimized by using a relatively short scan line (25 μm), which allowed us to acquire data at a high scan rate (2–3 ms per scan line) while preserving a nominal spatial resolution of 0.06 μm/pixel. Caged IP_3 was photolysed by ultraviolet light focused uniformly over a spot 200 μm in diameter surrounding the scan line (22). The stimulus strength was varied by regulating the flash duration with electronic shutter and/or changing light intensity via neutral density (ND) filters. We express stimulus strength on a linear relative scale calculated as $F_d/10^{ND}$, where F_d = flash duration in milliseconds and ND = optical density of the ND filters. Image data were processed in IDL (Research Systems; Boulder, CO) using custom-written software routines and exported to Microcal Origin, v. 6 (Northampton, MA) for analysis and graphing. Pearson's correlation coefficient (r) was used to determine the relationship between relative stimulus strength and specific response characteristics, and the Student's t-test was used to determine if two independent populations were significantly different ($p < 0.05$ required to achieve significance). Data are presented as mean ± SE.

Calculation of fluorescence ratio signals

A major goal of this study was to quantify the magnitudes of fluorescence signals during triggers and puffs as a basis for subsequent mathematical modeling. For this purpose we needed to correct the ''raw'' fluorescence measurements for artifactual distortions. The procedure is illustrated in Fig. 1, which diagrams the various factors contributing to the total fluorescence recorded from an oocyte. Fig. 1 *A* shows a raw fluorescence linescan image of two calcium puffs evoked by photoreleased IP_3, processed only by a 3 × 3 smoothing, and Fig. 1 *B* shows corresponding temporal profiles of fluorescence at the center of a puff (a), and at a location with no Ca^{2+} response (b). Fluorescence signals from nonratiometric indicators such as fluo-4 are conventionally expressed as ratios (F/F_0 or $\Delta F/F_0$) of the fluorescence (F) at each pixel relative to the mean resting fluorescence before stimulation (F_0).

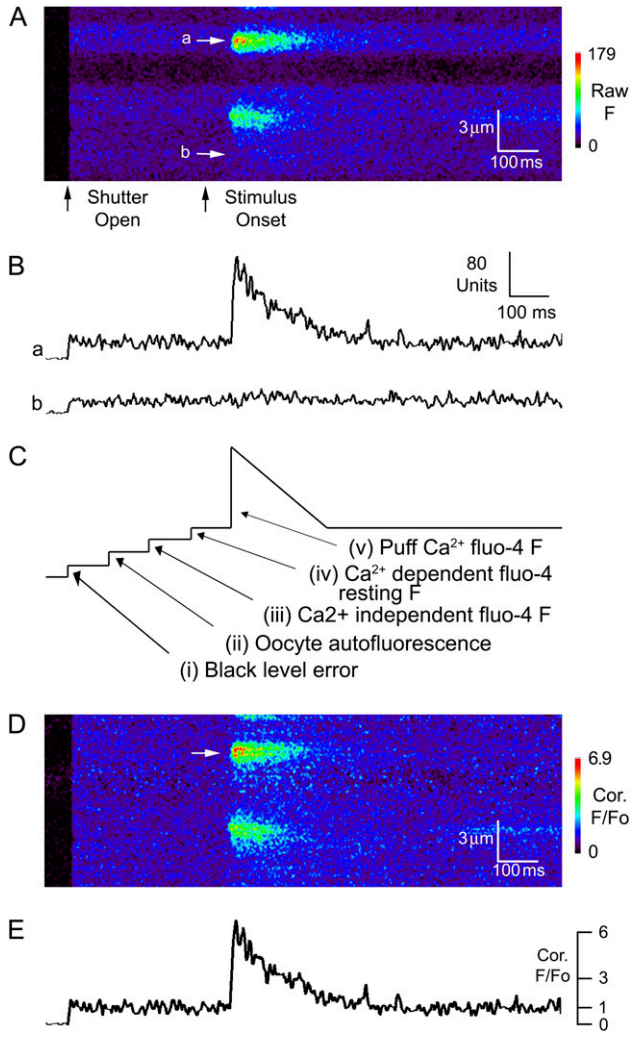

FIGURE 1 Confocal linescan imaging of Ca^{2+} puffs in *Xenopus* oocytes and factors contributing to the fluorescence signal. (*A*) Representative ''raw'' fluorescence image showing two puffs. Distance along the scan line is depicted vertically, and time runs from left to right. Increasing fluorescence (F) in arbitrary units on an 8-bit scale is depicted in pseudocolor as indicated by color bar. The shutter controlling the laser excitation light was opened when marked by the first arrow, and a photolysis flash was delivered to photorelease IP_3 at the second arrow. Data are unprocessed excepting a 3 × 3 pixel smoothing. (*B*) Temporal profile of raw fluorescence levels monitored at the two sites marked by white arrows in *A*. Measurements were averaged over three pixels (~0.2 μm). (*C*) Components contributing toward the total fluorescence signal at rest and during a puff: (*i*) photon and dark noise offset in the absence of laser excitation; (*ii*) oocyte autofluorescence; (*iii*) Ca^{2+}-independent fluorescence of indicator dye; (*iv*) Ca^{2+}-dependent fluorescence of indicator at basal cytosolic free [Ca^{2+}]; and Ca^{2+}-evoked fluorescence increase during a puff. Calculations of fluorescence ratio changes (F/F_0) were made after subtracting factors (*i*) and (*ii*) from the ''raw'' basal fluorescence to obtain a corrected value of F_0. Fluorescence steps and peak puff amplitude (*v*) are not to scale. Representative values (in raw fluorescence units) are $i = 2.5$, $ii = 2.0$, $iii = 2.9$, $iv = 19$, $v = 132$. (*D*) Pseudocolored fluorescence ratio image (F/F_0) derived from the record in *A* after correcting as described in *C*. (*E*) Temporal profile of the puff in *D* (*arrow*). The profile appears nearly identical to *B* but actually represents small critical differences for measuring small amplitude events, which will be the focus of this work. Timescale is the same as *D*.

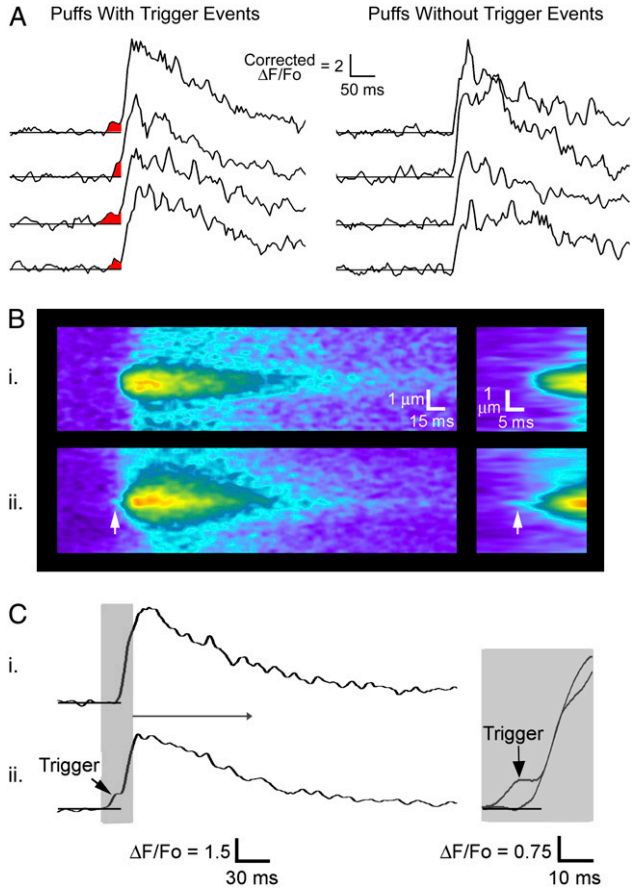

FIGURE 2 Ca^{2+} ''triggers'' preceding puffs. (*A*) Representative examples of puffs with (*left*) and without (*right*) trigger events. Triggers are highlighted by red shading. Traces show temporal profiles of fluorescence measured through the center of individual calcium puffs. (*B*) Averaged linescan images showing the temporal evolution of puffs without (*i*) and with (*ii*) preceding triggers. Images were formed after aligning individual puff images and represent averages of 12 events without triggers and 8 with triggers. Panels on the right show the rising phase of the puffs on an expanded timescale. (*C*). Temporal profiles taken through the centers of the averaged puffs shown in *B*. Panel on the right is an overlay of the puff rising phases, shown on expanded time and amplitude scales corresponding to the gray box in the main panel.

In the case of small fluorescence signals such as the triggers, errors in estimation of F_0 disproportionately affect calculation of $\Delta F/F_0$. To obtain a more accurate baseline fluorescence measurement representing only the fluo-4 fluorescence at basal free Ca^{2+} level, we subtracted artifactual signals contributed by i), shot noise and stray light in the detector, and ii), autofluorescence of the oocyte (Fig. 1 *C*).

First, the detector ''black level''was measured in each image file by recording before opening the laser shutter. As in our earlier publications using this microscope, the mean black level was subtracted from all subsequent measurements in that file. However, the resulting image file contains only positive integer values, thereby inadvertently introducing a small residual error because noise fluctuations above the mean are registered, whereas fluctuations below the mean are counted as zero. This was corrected here by subtracting the residual dark noise level from (floating point) temporal profiles of fluorescence. Second, we measured the autofluorescence of a subset of oocytes before loading with indicator dye under conditions (laser intensity, location in the oocyte) identical to those used for Ca^{2+} imaging. The mean autofluorescence was 2.0 ± 0.04 raw fluorescence units ($n = 43$ locations in 14 oocytes), and this value was subtracted from all image data before calculating fluorescence ratio images and corresponding temporal profiles, as illustrated in Fig. 1, *D* and *E*.

A remaining source of Ca^{2+}-independent fluorescence originates from the fluorescence of the indicator dye remaining at zero [Ca^{2+}] (Fig. 1 *C*). We estimated this by comparing the fluorescence of droplets of low-affinity fluo-4-dextran (25 μM, prepared from the same lot as that used for imaging; together with 100 mM KCl, 5 mM HEPES at pH 7.4) in Ca^{2+}-free medium (no added Ca^{2+} and 5 mM EGTA) and in saturating [Ca^{2+}] (100 μM $CaCl_2$). The residual fluorescence in Ca^{2+}-free medium was 2.2% of that in saturating Ca^{2+}. We did not apply any correction for Ca^{2+}-independent fluo-4 fluorescence here, but the value is important for the companion work where we model puff and trigger generation (20).

RESULTS

'Trigger' events often precede puffs

Puffs are believed to arise because CICR coordinates the concerted opening of several IP_3Rs within a cluster. It is likely, therefore, that a puff is initiated when Ca^{2+} liberated by the opening of a single IP_3R causes neighboring channels to open. In previous experiments we had failed to detect such putative single-channel trigger events (5,9) (but see Sun et al. (11) for first mention of possible trigger events). However, using higher-resolution imaging and a Ca^{2+} indicator dye (fluo-4-dextran) with high-dynamic range together with intracellular loading of EGTA to functionally uncouple puff sites (22), we now show that puffs do not always display a smoothly monotonic rising phase but in many instances are preceded by discrete brief low-amplitude events.

Representative examples of temporal profiles of individual puffs are shown in Fig. 2 *A*. Those on the left were selected as displaying trigger events (*red* shading), whereas those on the right show puffs that appear to rise monotonically from baseline without any detectable inflection in the rising phase. Fig. 2 *B* presents linescan images illustrating puffs without (i) and with (ii) trigger events, formed in both cases by averaging selected individual images after aligning puffs to their location of maximum intensity and time of maximal rate of rise, and Fig. 2 *C* shows temporal profiles of fluorescence ratio during these averaged events.

Given the brief duration and small amplitude of trigger events, we were concerned to exclude the possibility that they might be subjectively misidentified from random noise spikes that happened to precede a puff. Several observations argue against that possibility. First, the amplitudes of triggers were generally above the baseline noise level, even in individual traces (Fig. 2 *A*) and were much larger than baseline noise after averaging several events (Fig. 2 *C*). Second, if the triggers simply represented upward noise spikes, then puffs selected as failing to show triggers would be expected to display a corresponding initial negative deflection—which was not the case (Fig. 2, *A* and *C*). Third, distinct inflections in the rising phase were still apparent in time-aligned averages of randomly selected puffs (e.g., *inset* to Fig. 3), where only a portion of the averaged puffs had trigger events.

The question then arises as to whether these small Ca^{2+} signals are specifically associated with puffs or whether we identify triggers as random events that coincidentally arise at the start of a puff. We addressed this by counting the number of times upward baseline fluctuations exceeded a threshold of 1 $\Delta F/F_0$ (the amplitude of an average-sized trigger) for ≥4 ms in 12-ms bins immediately preceding puff onset and at sequentially earlier times. Trigger events exceeding this threshold were seen immediately preceding 75% (8/12) of unselected puffs evoked by weak stimuli (see below), whereas we observed no corresponding random events at earlier times (0/96 time bins).

Fraction of puffs preceded by triggers

Pooled data over a range of stimulus intensities revealed that ~40% of all puffs were preceded by detectable trigger events. To further examine whether the likelihood of observing trigger events varies with concentration of IP_3, we determined the percentage of puffs displaying triggers after photolysis flashes of varying strengths. As shown in Fig. 3, most puffs (~80%) evoked by weak flashes were preceded by detectable triggers, but this proportion declined to <50% with stronger stimuli. To reduce subjective bias, the observer was blind to the stimulus strength when determining which puffs had triggers. Moreover, averages of randomly selected puffs after weak stimuli showed a clear trigger event, whereas a trigger event was barely discernable in an ensemble average of unselected puffs evoked by intermediate stimuli where only ~20% of puffs showed triggers (*inset*, Fig. 3).

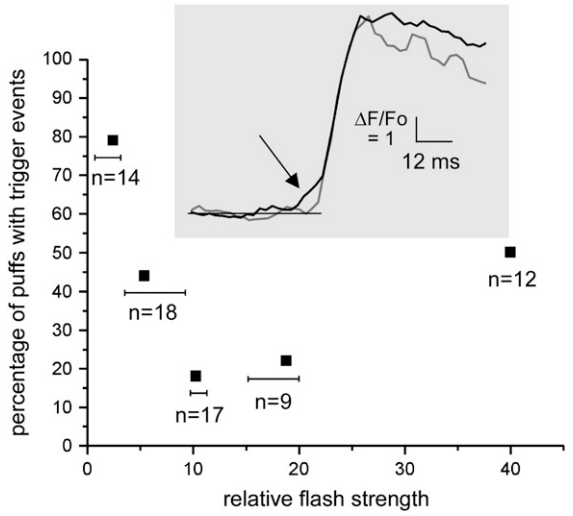

FIGURE 3 Proportion of puffs preceded by triggers varies with amount of photoreleased IP_3. Graph shows the percentage of puffs showing detectable triggers as a function of relative photolysis flash strength. Data were grouped across ranges of flash strengths as marked by the horizontal bars, and the numbers of events in each group are indicated. The inset shows averages of 12 puffs evoked by the weakest stimulus intensities (*solid line*, *arrow* points to average trigger event, relative stimulus strength of 2.37 ± 0.01) and of 11 puffs generated by higher stimulus intensities (*shaded line*, relative stimulus strength of 11.28 ± 0.71). Both averages were formed from unselected events; i.e., without regard to the presence of triggers.

Relative amplitudes of puffs and triggers

Ninety-two calcium puffs (48 with trigger events and 44 without) were selected for analysis of the spatial and temporal characteristics of the triggers and puffs. Table 1 summarizes average values of their fluorescence ratio amplitudes, spatial widths at half peak amplitude, and durations.

Fig. 4 *A* shows a scatter plot of corrected trigger amplitude ($\Delta F/F_0$; measured at the point of inflection before the rapid rate of rise of a puff) as a function of relative flash strength. No correlation was apparent ($r = 0.15$; slope of linear regression = 0.01 ± 0.01; $n = 29$), and we pooled data from all flash strengths to derive the amplitude distribution of triggers (Fig. 4 *B*), yielding a mean amplitude $\Delta F/F_0 = 1.26 \pm 0.10$ ($n = 48$). The peak amplitudes of puffs (including events both with and without triggers) also showed only a weakly positive correlation with flash strength (Fig. 4 *C*, $r = 0.37$; slope = 0.09 ± 0.03; $n = 73$). We thus pooled data across different flash strengths to obtain the distribution of puff amplitudes (Fig. 4 *D*; mean $\Delta F/F_0 = 7.3 \pm 0.35$, $n = 92$).

Measurements were made using fluo-4-dextrans to simultaneously resolve trigger events and puffs, but the relatively high affinity of these indicators introduced concern that the fluorescence signal may have approached saturation during the much larger puffs. To exclude this possibility, puff amplitudes were separately measured using a low-affinity calcium indicator (Oregon Green 5N; $K_d = 20\ \mu M$). This again revealed only a weakly positive correlation between puff amplitude and flash strength ($r = 0.46$; slope = 0.01 ± 0.003; $n = 57$; data not shown), indicating that the maximal Ca^{2+} concentration attained during a puff indeed shows relatively little dependence on [IP_3]. Trigger events were not resolved with Oregon Green 5N.

To use the trigger events as a yardstick by which to estimate the minimum number of channels opening during a puff, we calculated the puff/trigger amplitude ratios from

TABLE 1 Average amplitude, spatial, and kinetic characteristics of puffs and triggers

	Puff	Trigger
Amplitude (corrected)	7.27 ± 0.35 $\Delta F/F_0$ $n = 92$	1.26 ± 0.10 $\Delta F/F_0$ $n = 48$
Puff rise time or trigger duration	18.97 ± 0.79 ms $n = 92$	11.74 ± 0.65 ms $n = 48$
FWHA	1.51 ± 0.05 μm $n = 92$	0.57 ± 0.09 μm $n = 22$
FDHA	70.14 ± 3.11 ms $n = 92$	

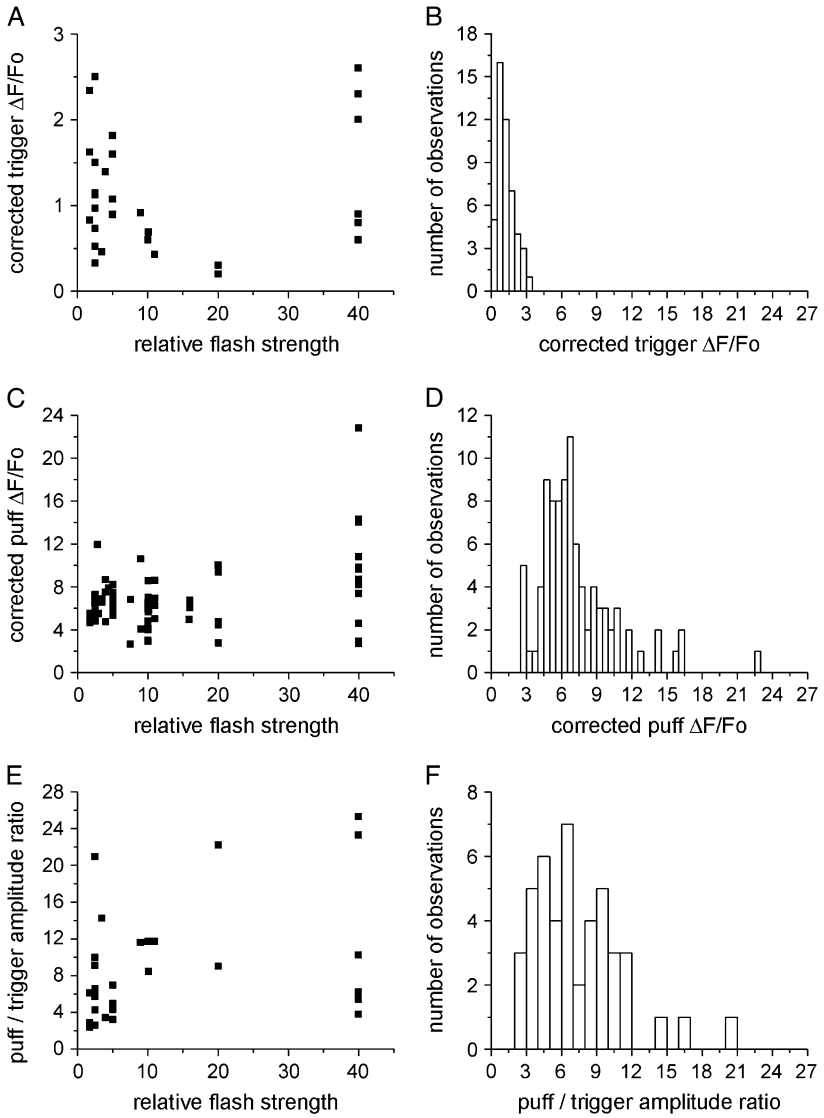

FIGURE 4 Corrected fluorescence amplitudes of triggers and puffs. (*A* and *C*) Scatterplots show the respective peak amplitudes of triggers and puffs as a function of relative flash strength. (*B* and *D*) Histograms showing the corresponding distributions of trigger and puff amplitudes, obtained after pooling measurements across all stimulus strengths. The histograms include data from experiments additional to those in *A* and *C*, where stimulus intensity was not quantified (total $n = 48$ triggers and 92 puffs). (*E*) Ratios of puff/trigger amplitude derived from paired measurements on 29 puffs as a function of flash duration. (*F*). Distribution histogram of puff/trigger amplitude ratios derived from paired measurements on 48 puffs.

paired measurements on puffs that displayed triggers. The distribution of ratios is plotted in Fig. 4 *F*, and the ratio showed no obvious correlation with flash strength (Fig. 4 *E*; $r = 0.37$; slope $= 0.16 \pm 0.08$; $n = 29$). The mean puff/trigger ratio derived from paired individual measurements was 8.44 ± 0.78 ($n = 48$); but this value is likely to be exaggerated by instances where very small trigger amplitudes gave rise to large ratios. Thus, we calculated a more reliable estimate of the puff/trigger amplitude ratio from the average puff and trigger amplitudes, yielding a value of 5.8.

Trigger and puff kinetics

Trigger durations were measured from the apparent onset of the trigger event to the start of the fast rise of the puff. The distribution of trigger durations ranged between ~5 ms and 25 ms (Fig. 5 *B*), and there was no apparent dependence of trigger duration on flash strength (Fig. 5 *A*; $r = -0.01$; slope $= -0.003 \pm 0.05$; $n = 29$). The average trigger duration was 11.7 ± 0.6 ms ($n = 48$). Puff rise times were measured from the beginning of the puff onset (or the end of the trigger event in those with triggers) until the time when the puff reached ~95% peak amplitude. Again, there was no significant dependence of puff rise time on relative flash strength (Fig. 5 *C*; $r = -0.15$; slope $= -0.10 \pm 0.07$; $n = 73$), and the distribution of rise times (Fig. 5 *D*) gave a mean of 19.0 ± 0.80 ms, $n = 92$. Puff durations were measured as full duration at half peak amplitude (FDHA). There was a weak negative correlation between FDHA and relative flash strength (Fig. 5 *E*; $r = -0.30$; slope $= -0.62 \pm 0.24$; $n = 73$), and the distribution of all values is shown in Fig. 5 *F*. The mean FDHA was 70.1 ± 3.1 ms, $n = 92$.

Spatial distribution of fluorescence signal during triggers and puffs

Fig. 6 *A* shows averaged spatial profiles derived from representative puffs and trigger events. Because the baseline

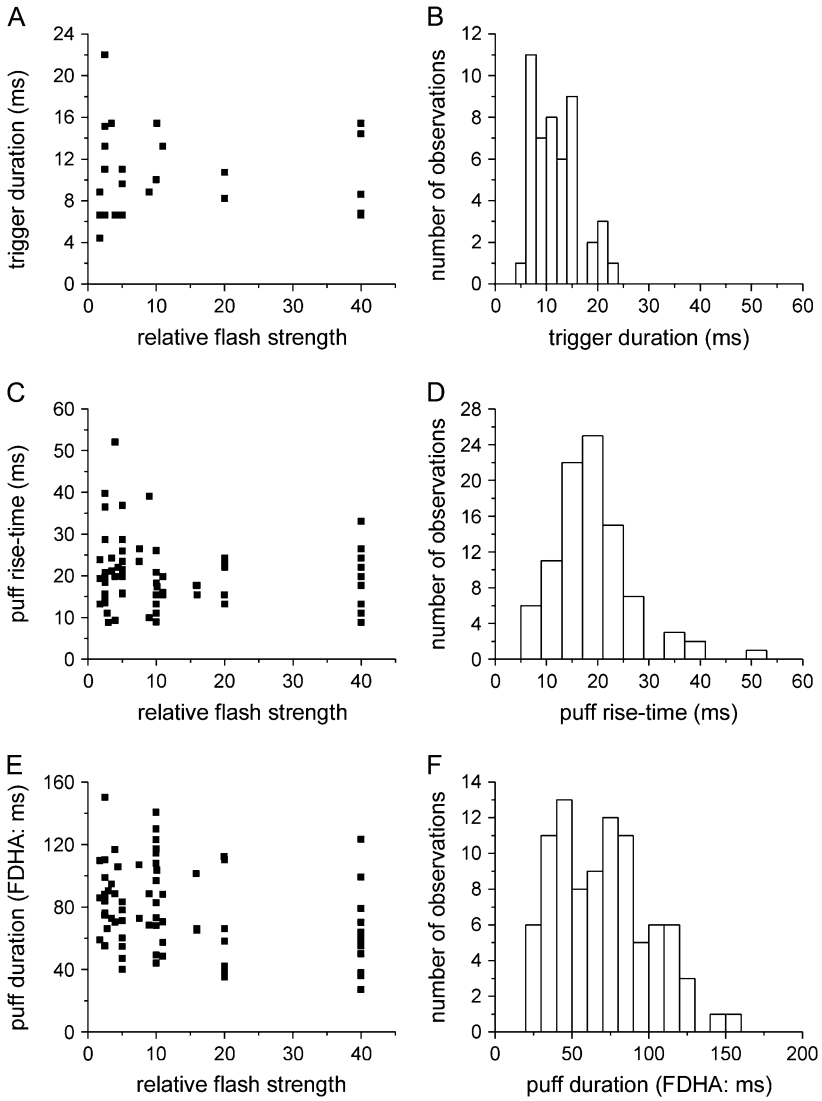

FIGURE 5 Temporal characteristics of puffs and trigger events. (*A*, *C*, *E*) Scatterplots showing the relationship between photolysis stimulus strengths and duration of trigger events ($n = 29$), puff rise time ($n = 73$), and puff FDHA ($n = 73$). (*B*, *D*, *F*) Histograms showing the respective distributions of trigger durations ($n = 48$), puff rise times ($n = 92$), and puff durations (FDHA; $n = 92$). Data were pooled across all stimulus strengths and include measurements from additional puffs and triggers not shown in the scatterplots.

noise level was appreciable in relation to the amplitude of triggers, we were able to obtain reliable measurements of trigger width (FWHA) from only a subset of events (Fig. 6 *B*; $n = 22$), yielding a mean width of 0.57 ± 0.09 μm. Puff widths measured in the same way showed no dependence ($r = -0.07$; slope = −0.003 ± 0.03; $n = 73$) on photolysis flash strength (Fig. 6 *C*), and pooled measurements displayed a roughly Gaussian distribution of puff widths (Fig. 6 *D*), with a mean of 1.51 ± 0.05 μm ($n = 92$); almost three times wider than trigger events.

Are puffs with triggers the same as puffs without triggers?

The mean corrected amplitude of puffs with trigger events (7.46 ± 0.71 $\Delta F/F_0$; $n = 30$) tended to be greater than events without detectable triggers (6.06 ± 0.34 $\Delta F/F_0$; $n = 38$); but the difference just failed to reach statistical significance ($p = 0.06$). No significant differences were apparent in puff widths (puffs with trigger = 1.42 ± 0.09 μm, $n = 30$; without trigger = 1.56 ± 0.09 μm, $n = 38$; $p = 0.25$), durations (FDHA of puffs with trigger = 73.94 ± 4.81 ms, $n = 30$; without trigger = 84.15 ± 4.47; $p = 0.13$), or rise times (19.86 ± 1.32 ms, $n = 30$ vs. 19.79 ± 1.46 ms, $n = 38$; $p = 0.97$).

DISCUSSION

We show that IP_3-evoked Ca^{2+} puffs in *Xenopus* oocytes are often preceded by brief, small amplitude Ca^{2+} signals, which we name ''trigger'' events. Although both puffs and trigger events exhibit variability in their spatial and temporal characteristics, these characteristics are largely independent of IP_3 concentration. As discussed below, the trigger events most probably represent the opening of a single IP_3R/ channel and thus provide a useful yardstick by which to estimate the number and spatial distribution of IP_3Rs involved in an average puff (20) and provide clues as to the mechanism of puff initiation.

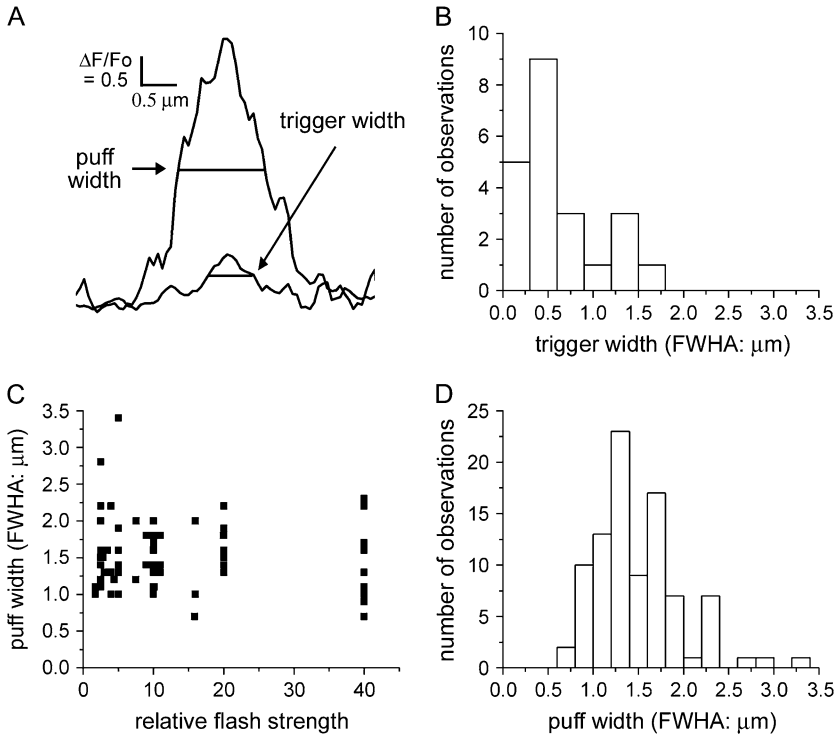

FIGURE 6 Spatial profile of puffs and triggers. Trigger events are much narrower than puffs. (*A*) Averaged spatial profiles derived from 10 puffs and 10 trigger events, showing measurement of FWHA. Individual profiles were obtained by measuring the fluorescence distribution along the scan line, averaged over three time points (6.6 ms), at times corresponding to the peak of the trigger events (just before the inflection to the rapid rising phase of the puff) and at the peak of the puff. (*B*) Distribution of trigger widths. Data are from a subset of trigger events ($n = 22$), as in many instances the baseline noise precluded measurement. (*C*) Puff width at half peak amplitude (FWHA; $n = 73$) is independent of photolysis flash strength. (*D*) Distribution of FWHA of puffs, pooled across all stimulus intensities ($n = 92$).

Trigger events likely represent single IP_3R channel openings

Our experiments were done using fluo-4 dextran as the Ca^{2+} indicator because its fluorescence in the absence of calcium is extremely low but increases >30-fold upon binding calcium. This large dynamic range, together with fast (2 ms per line) confocal imaging allowed us to resolve trigger events preceding puffs, whereas previous attempts to identify such ''pacemaker'' activity during the rising phase of puffs had failed (5).

Several observations suggest that the trigger events likely represent the initial opening of a single IP_3R channel. Most directly, fluorescence signals generated by Ca^{2+} flux through individual N-type voltage-gated channels, expressed in oocytes and imaged with the same indicator and microscope system as used here, showed amplitudes ($\Delta F/F_0$ 1–2) and spatial widths (FWHM 0.55–0.7 μm) similar to the trigger events (23). The Ca^{2+} currents through the N-type channels were ~0.3 pA, which is comparable to or smaller than the current (~0.5 pA) estimated to pass through the IP_3R channel under physiological conditions (24). Moreover, modeling simulations that take into account factors including cytosolic Ca^{2+} buffering and the microscope point-spread function also indicate that the trigger events are consistent with an underlying Ca^{2+} flux equivalent to a single-channel current of 0.3–0.5 pA (20,25). The mean channel open dwell time derived from patch-clamp measurements of IP_3R in *Xenopus* oocyte nuclei is ~6 ms (26), so it might well be that triggers arise from a single opening event, given that our measure of the mean trigger duration (12 ms) is probably overestimated owing to a failure to resolve brief signals. Alternatively, the trigger may represent a burst of repeated openings with an overall high open probability, whereby repetitive opening of a single-channel results from positive feedback by Ca^{2+} passing through that channel (27).

How many IP_3R channels open during a puff?

Strong evidence indicates that Ca^{2+} puffs arise through the concerted opening of IP_3Rs arranged in clusters (5,7,10,12). However, experimental data have still not fully resolved questions regarding how many channels are in a cluster, how many of those channels open during a puff, and the spacing between IP_3Rs; although these issues have been addressed in modeling studies (8,28). By comparing the characteristics of a presumptive single IP_3R/channel opening (trigger) to the opening of many channels (a puff) at the same site, we are in a unique position to estimate such parameters. Given that the mean puff fluorescence amplitude is 5.8 times greater than that of triggers (Table 1), we can conclude that at least six channels open during a puff.

However, calculating the potential channel number based upon a puff/trigger amplitude ratio alone is clearly simplistic and assumes a linear superposition of channel signals, which is likely not the case. An alternative method, which is less sensitive to local indicator saturation, is to estimate the respective Ca^{2+} fluxes (currents) underlying both the trigger and puff by determining the fluorescence ''signal mass'' (fluorescence ratio change × volume) of each event (11). Here, we followed the procedure of Hollingworth et al. (29)

and calculated signal mass as peak fluorescence ratio × 1.2 × the cube of the width (FWHA) of a Gaussian function fitted to the distribution of fluorescence along the scan line at the peak of the event. The mean signal mass of the puff and trigger was then divided, respectively, by the average puff rise time and trigger duration to obtain a relative measure of calcium flux during each of these events. This yielded an average puff/trigger flux ratio of ~60. However, this estimate is subject to considerable uncertainties, in particular because of the large errors introduced by cubing what is already an uncertain measurement of the width of the small trigger events.

The problems associated with both of these methods led us to consider a more complex deterministic mathematical model (20) incorporating the major variables involved in calcium release from single and multiple channels. By using the experimental values described in this work in conjunction with consideration of other factors such as intracellular buffers and the relationship between actual calcium ions released and the confocal signal observed, we show in a companion work that a few tens of channels likely open during a puff (20).

Blips, trigger events, and the initiation of puffs

IP_3R-mediated Ca^{2+} ''blips'' have been described previously (9–11) and are generally observed temporally separate from puffs, yet often at the same locations (11). This study marks the first time, to our knowledge, that these putative single-channel Ca^{2+} events are consistently observed as precursors to puffs. We propose that these trigger events are the foundation on which puffs are initiated and built, and as such they should prove helpful for determining the mechanisms underlying intracellular calcium signaling.

Opening of IP_3Rs/channels requires the presence of both IP_3 and calcium (2,4). At basal [Ca^{2+}] and at the relatively small IP_3 concentrations used here to evoke puffs, the probability of any individual IP_3R channel becoming activated will be very low. When such an event does occur, we hypothesize that the channel may either i), open once, or as a burst of several openings sustained by Ca^{2+} flux through the channel, but then terminate when IP_3 dissociates, to generate a discrete blip; or ii), trigger the regenerative opening by CICR of neighboring channels within the cluster to generate a puff. The observations of trigger events with durations of 10 ms or longer suggest that the functional coupling between IP_3Rs in a cluster is relatively weak, so that the enormous Ca^{2+} microdomain in the immediate vicinity of an open channel does not invariably evoke an immediate regenerative opening of multiple adjacent channels. On the other hand, a majority of puffs evoked by higher [IP_3] showed an abrupt rising phase, without discernable triggers. In these cases, it may be that the latency between opening of an initial channel and regenerative triggering of CICR became too short to resolve because a greater number of channels had bound IP_3 and were thereby in an ''activatable'' state. It remains to be determined to what extent the coupling efficiency is limited by the spacing between IP_3Rs or by their inherent kinetics of channel opening after binding of activating Ca^{2+}.

Trigger events were followed by a rapid inflection into the rising phase of the puff proper, with a mean duration of ~19 ms from the time of inflection to the peak of the puff. Most puffs showed a smooth, monotonic rising phase after the trigger. However, a small subset did have slower, ''step-like'' onsets that might correspond to the successive recruitment of IP_3R channels. Because the number of such events was small and there are potential confounding interpretations (e.g., out of focus fluorescence also will show a slower rate of rise), we did not attempt to analyze this limited subset of data. In general, the regenerative recruitment of channels appears to proceed rapidly once more than one channel is open, and the release process already begins to terminate after ~20 ms.

Puff characteristics are relatively independent of [IP_3]

The amplitude, spatial spread, and duration of puffs all showed only a slight dependence on the amount of photoreleased IP_3, in agreement with earlier findings (30) that local IP_3-evoked Ca^{2+} liberation approximates an ''all-or-none'' process. On the other hand, the probability of puff occurrence grew steeply as a function of increasing photorelease (14), as would be expected if a greater number of IP_3Rs within a cluster bound IP_3, thereby increasing the likelihood that one would open after the random binding of a Ca^{2+} ion and trigger a puff. The cumulative Ca^{2+} liberation during a puff seems, therefore, not to be delimited simply by the extent of IP_3 binding to receptors in a cluster but, instead, may involve some negative feedback mechanism—possibly including inhibition by locally elevated cytosolic Ca^{2+} or by depletion of luminal [Ca^{2+}]. Although puff parameters showed little average dependence on the amount of photoreleased IP_3, there was still considerable variability in puff amplitudes and durations between individual events, probably reflecting both stochastic variations in the numbers and kinetics open IP_3R channels and differences in IP_3R number and distribution among different puff sites (11).

Comparison with RyR-mediated Ca^{2+} signals

The hierarchy of IP_3-evoked Ca^{2+} signals encompassing single-channel events (blips, triggers), multi-channel events (puffs), and global cell waves (10,11) is closely replicated in muscle and other cells where RyRs mediate CICR from the sarco/endoplasmic reticulum. Thus, analogous to puffs, Ca^{2+} ''sparks'' are now generally believed to arise from the concerted opening of several clustered RyRs (31), whereas smaller events (''quarks'') (10,32) are thought to be generated

by the opening of one, or a small number of, RyRs. Of particular interest here are the Ca^{2+} ''embers'', which were originally described as faint tails after sparks in frog skeletal muscle (32) but are more prevalent in rat muscle where they are seen to precede as well as trail a fraction of spontaneous sparks (32). Thus, the trigger and ember events are likely to continue to provide important insights into the fundamental mechanisms involved in initiation of the elementary puffs and sparks from which Ca^{2+} signals are constructed in numerous cell types.

This work was supported by grants GM 48071 and GM 65830 from the National Institutes of Health.

REFERENCES

1. Berridge, M. J. 1993. Inositol trisphosphate and calcium signalling. *Nature*. 361:315–325.
2. Iino, M. 1990. Biphasic Ca^{2+} dependence of inositol 1,4,5-trisphosphate-induced Ca release in smooth muscle cells of the guinea pig *taenia caeci*. *J. Gen. Physiol.* 95:1103–1122.
3. Finch, E. A., T. J. Turner, and S. M. Goldin. 1991. Calcium as a coagonist of inositol 1,4,5-trisphosphate-induced calcium release. *Science*. 252:443–446.
4. Bezprozvanny, I., J. Watras, and B. E. Ehrlich. 1991. Bell-shaped calcium-response curves of Ins(1,4,5)P_3- and calcium-gated channels from endoplasmic reticulum of cerebellum. *Nature*. 351:751–754.
5. Yao, Y., J. Choi, and I. Parker. 1995. Quantal puffs of intracellular Ca^{2+} evoked by inositol trisphosphate in *Xenopus* oocytes. *J. Physiol.* 482:533–553.
6. Callamaras, N., and I. Parker. 1994. Inositol 1,4,5-trisphosphate receptors in *Xenopus laevis* oocytes: localization and modulation by Ca^{2+}. *Cell Calcium*. 15:66–78.
7. Mak, D. O., and J. K. Foskett. 1997. Single-channel kinetics, inactivation, and spatial distribution of inositol trisphosphate (IP_3) receptors in *Xenopus* oocyte nucleus. *J. Gen. Physiol.* 109:571–587.
8. Shuai, J. W., and P. Jung. 2003. Optimal ion channel clustering for intracellular calcium signaling. *Proc. Natl. Acad. Sci. USA*. 100:506–510.
9. Parker, I., and Y. Yao. 1996. Ca^{2+} transients associated with openings of inositol trisphosphate-gated channels in *Xenopus* oocytes. *J. Physiol.* 491:663–668.
10. Bootman, M., E. Niggli, M. Berridge, and P. Lipp. 1997. Imaging the hierarchical Ca^{2+} signalling system in HeLa cells. *J. Physiol.* 499:307–314.
11. Sun, X. P., N. Callamaras, J. S. Marchant, and I. Parker. 1998. A continuum of $InsP_3$-mediated elementary Ca^{2+} signalling events in *Xenopus* oocytes. *J. Physiol.* 509:67–80.
12. Parker, I., and Y. Yao. 1991. Regenerative release of calcium from functionally discrete subcellular stores by inositol trisphosphate. *Proc. Biol. Sci.* 246:269–274.
13. Parker, I., J. Choi, and Y. Yao. 1996. Elementary events of $InsP_3$-induced Ca2+ liberation in *Xenopus* oocytes: hot spots, puffs and blips. *Cell Calcium.* 20:105–121.
14. Callamaras, N., J. S. Marchant, X. P. Sun, and I. Parker. 1998. Activation and co-ordination of $InsP_3$-mediated elementary Ca^{2+} events during global Ca^{2+} signals in *Xenopus* oocytes. *J. Physiol.* 509:81–91.
15. Busa, W. B., J. E. Ferguson, S. K. Joseph, J. R. Williamson, and R. Nuccitelli. 1985. Activation of frog (*Xenopus laevis*) eggs by inositol trisphosphate. I. Characterization of Ca^{2+} release from intracellular stores. *J. Cell Biol.* 101:677–682.
16. Parker, I., and R. Miledi. 1986. Changes in intracellular calcium and in membrane currents evoked by injection of inositol trisphosphate into *Xenopus* oocytes. *Proc. R. Soc. Lond. B Biol. Sci.* 228:307–315.
17. DeLisle, S., and M. J. Welsh. 1992. Inositol trisphosphate is required for the propagation of calcium waves in *Xenopus* oocytes. *J. Biol. Chem.* 267:7963–7966.
18. Lechleiter, J. D., and D. E. Clapham. 1992. Molecular mechanisms of intracellular calcium excitability in *X. laevis* oocytes. *Cell*. 69: 283–294.
19. Parys, J. B., S. W. Sernett, S. DeLisle, P. M. Snyder, M. J. Welsh, and K. P. Campbell. 1992. Isolation, characterization, and localization of the inositol 1,4,5-trisphosphate receptor protein in *Xenopus laevis* oocytes. *J. Biol. Chem.* 267:18776–18782.
20. Shuai, J., H. J. Rose, and I. Parker. 2006. The number and spatial distribution of IP_3 receptors underlying calcium puffs in *Xenopus* oocytes. *Biophys. J.* 91:4033–4044.
21. Callamaras, N., and I. Parker. 2000. Phasic characteristic of elementary Ca^{2+} release sites underlies quantal responses to IP_3. *EMBO J.* 19: 3608–3617.
22. Parker, I., N. Callamaras, and W. G. Wier. 1997. A high-resolution, confocal laser-scanning microscope and flash photolysis system for physiological studies. *Cell Calcium.* 21:441–452.
23. Demuro, A., and I. Parker. 2003. Optical single-channel recording: imaging Ca^{2+} flux through individual N-type voltage-gated channels expressed in *Xenopus* oocytes. *Cell Calcium.* 34:499–509.
24. Bezprozvanny, I., and B. E. Ehrlich. 1994. Inositol (1,4,5)-trisphosphate ($InsP_3$)-gated Ca channels from cerebellum: conduction properties for divalent cations and regulation by intraluminal calcium. *J. Gen. Physiol.* 104:821–856.
25. Shuai, J., and I. Parker. 2005. Optical single-channel recording by imaging Ca^{2+} flux through individual ion channels: theoretical considerations and limits to resolution. *Cell Calcium.* 37:283–299.
26. Mak, D. O., S. McBride, and J. K. Foskett. 2001. ATP-dependent adenophostin activation of inositol 1,4,5-trisphosphate receptor channel gating: kinetic implications for the durations of calcium puffs in cells. *J. Gen. Physiol.* 117:299–314.
27. Swillens, S., P. Champeil, L. Combettes, and G. Dupont. 1998. Stochastic simulation of a single inositol 1,4,5-trisphosphate-sensitive Ca^{2+} channel reveals repetitive openings during 'blip-like' Ca^{2+} transients. *Cell Calcium.* 23:291–302.
28. Swillens, S., G. Dupont, L. Combettes, and P. Champeil. 1999. From calcium blips to calcium puffs: theoretical analysis of the requirements for interchannel communication. *Proc. Natl. Acad. Sci. USA*. 96:13750–13755.
29. Hollingworth, S., J. Peet, W. K. Chandler, and S. M. Baylor. 2001. Calcium sparks in intact skeletal muscle fibers of the frog. *J. Gen. Physiol.* 118:653–678.
30. Parker, I., and I. Ivorra. 1990. Localized all-or-none calcium liberation by inositol trisphosphate. *Science*. 250:977–979.
31. Rios, E., and G. Brum. 2002. Ca^{2+} release flux underlying Ca^{2+} transients and Ca^{2+} sparks in skeletal muscle. *Front. Biosci.* 7:d1195–d1211.
32. Zhou, J., G. Brum, A. Gonzalez, B. S. Launikonis, M. D. Stern, and E. Rios. 2003. Ca^{2+} sparks and embers of mammalian muscle. Properties of the sources. *J. Gen. Physiol.* 122:95–114.